

A review of variable-impedance acoustic liner concepts developed at NASA

Michael G. Jones[1]
NASA Langley Research Center
Hampton, VA 23681-2199

ABSTRACT

This paper presents results attained in the NASA Langley Research Center test rigs using acoustic liners for which the impedance varies over the liner surface. These liners are typically designed for significant sound absorption over a wide frequency range, but it is also possible to design them to achieve increased absorption at selected frequencies. A brief review is provided regarding a number of variable-impedance concepts. The first is a modified version of a conventional two-layer liner, in which the embedded septum location and flow resistance are different for adjacent core chambers. Two concepts employ core chambers with different lengths, one with bent chambers to allow packaging within a limited volume, and the other with shared inlet ports to reduce the surface porosity. The last concept employs a perforated facesheet in which the hole diameter and porosity are varied over the surface of the liner. Data acquired in the NASA normal incidence and grazing flow impedance tubes are used to demonstrate the capabilities of these concepts. Impedance prediction models are also presented for comparison with these measured data.

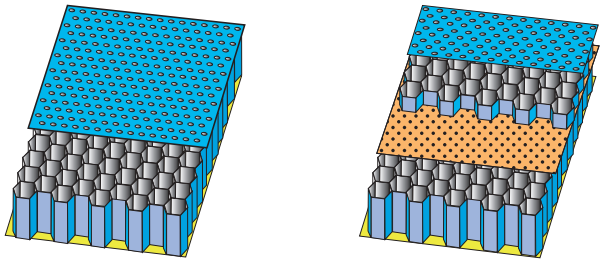
[1]**michael.g.jones@nasa.gov**

1. INTRODUCTION

Acoustic liners are passive devices typically mounted in the walls of aircraft inlets and aft-bypass ducts to absorb noise generated by the fan. Single-degree-of-freedom (SDOF) and two-degree-of-freedom (2DOF) perforate-over-honeycomb liners (see Figure 1) have been used on commercial aircraft since the early 1950's [1]. SDOF liners are generally excellent narrow-band sound absorbers, while 2DOF liners provide increased broadband sound absorption at the expense of reduced tonal absorption. The key parameter used to characterize acoustic liners is acoustic impedance, ζ, defined as the ratio of the Fourier transforms of the acoustic pressure, p, and the normal component of acoustic particle velocity, u_N, at a point of interest (e.g., at the surface of the liner) [2]. This impedance is commonly represented as

$$\zeta = \frac{p}{\rho c u_N} = \theta + \mathrm{i}\chi. \tag{1}$$

This impedance (assumed normalized by the characteristic impedance of air, ρc, where ρ and c represent the local density and sound speed of air, respectively) is a function of frequency, the liner geometry, and the aeroacoustic environment.



(a) SDOF. (b) 2DOF.

Figure 1: Sketches of SDOF and 2DOF liners.

The noise radiated from current high bypass-ratio, commercial aircraft engine nacelles consists of a strong broadband noise spectrum and significant tonal content. This tonal content is often at the blade passage frequency (and harmonics), which can be at low frequencies due to the larger fan diameter associated with the increased bypass ratio.

As a result, there is a need for acoustic liners specifically designed for low frequency and broadband sound reduction. The liner physics team at NASA Langley Research Center has explored a number of liner concepts for which the impedance is varied over the liner surface. Depending on the specific design features, these liners can be tuned to target either or both of these conditions.

This paper presents results for a few of these variable-impedance liner concepts. Impedance prediction models are presented first, followed by discussions for four variable-impedance acoustic liner concepts and a summary of the key contributions of this research.

2. IMPEDANCE PREDICTION MODELS

The surface impedance for most of the liner configurations presented in this paper can be predicted using the Two-Parameter Model, TPM [3,4] and a transmission line model, ZKTL [5, 6].

2.1. Two-Parameter Model

The TPM is used to predict the surface impedance of SDOF liners in the presence of tangential mean flow. The acoustic impedance of the liner is given by

$$\zeta = \frac{32\mu t}{\rho c\left(\sigma C_D\right) d^2} + \frac{1}{2c\left(\sigma C_D\right)^2} u_{\text{rms}} + \frac{M_{\text{C/L}}}{\sigma\left\{2 + 1.256\left(\delta_1/d\right)\right\}} + \text{i}\left\{\frac{k(t+\epsilon d)}{\sigma C_D} - \cot\left(kh\right)\right\}, \quad (2)$$

where t, d, and σ repesent the thickness, hole diameter, and open area ratio of the facesheet, and μ, C_D, $M_{\text{C/L}}$, and δ_1 are the viscosity of air, discharge coefficient, centerline Mach number, and boundary layer displacement thickness, respectively. The freespace wavenumber and RMS acoustic particle velocity are given by k and u_{rms}. Finally, h represents the core depth and ϵd is an end correction (nominal value of 0.85).

2.2. ZKTL Model

The ZKTL model treats each portion (air gap and perforated sheet) of the liner chamber sequentially (see Figure 2). For a rigid and impervious backplate, the normalized acoustic pressure and particle velocity are given by $p_0 = 1$ and $u_0 = 0$ (acoustic pressures and particle velocities are normalized by ρc^2 and c).

Changes in the acoustic pressure and particle velocity across the air gap with height h are computed via

$$\left(\begin{array}{c} p_1 \\ u_1 \end{array}\right) = \left(\begin{array}{cc} T_{11} & T_{12} \\ T_{21} & T_{22} \end{array}\right)\left(\begin{array}{c} p_0 \\ u_0 \end{array}\right), \text{ where } \left\{\begin{array}{l} T_{11} = T_{22} = \cosh(k\Gamma h) \\ T_{12} = \zeta_c \sinh(k\Gamma h) \\ T_{21} = \zeta_c^{-1} \sinh(k\Gamma h) \end{array}\right\}. \quad (3)$$

Using a low reduced-frequency solution provided by Zwikker and Kosten [7] as an initial estimate, Tijdeman [8] suggested the propagation constant, Γ, and characteristic impedance, ζ_c, could be computed as

$$\Gamma = \sqrt{\frac{J_0(\mathrm{i}^{3/2}s)}{J_2(\mathrm{i}^{3/2}s)}}\sqrt{\frac{\gamma}{n_\Gamma}}, \qquad \zeta_c = \frac{-\mathrm{i}}{\Gamma}\frac{J_0(\mathrm{i}^{3/2}s)}{J_2(\mathrm{i}^{3/2}s)}, \tag{4}$$

where J_0 and J_2 are Bessel functions, $i = \sqrt{-1}$, and

$$s = \frac{d_c}{2}\sqrt{\frac{\rho_s\omega}{\mu}}, \; \gamma = \frac{C_p}{C_v}, \; n_\Gamma = \left[1 + \frac{\gamma - 1}{\gamma}\frac{J_0(\mathrm{i}^{3/2}P_r^{1/2}s)}{J_0(\mathrm{i}^{3/2}P_r^{1/2}s)}\right]^{-1}, \; P_r = \frac{\mu C_p}{\kappa}. \tag{5}$$

The parameters used in these equations include the shear wave number, s, the chamber diameter, d_c, the static density, ρ_s, the angular frequency, ω, the Prandtl number, P_r, the specific heat at constant pressure and volume, C_p and C_v, and the thermal conductivity of gas in the chamber, κ.

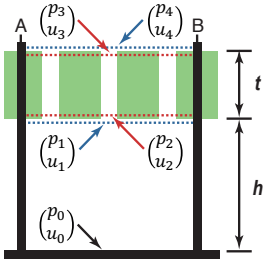


Figure 2: Sketch of single chamber for transmision line impedance prediction model.

The acoustic pressure and acoustic mass flow are assumed to be constant across the $\{1, 2\}$ interface in Figure 2, such that $p_2 = p_1$ and $N_p S_p u_2 = S_c u_1$, where N_p is the number of perforates (3 in this example) connected to a single air cavity, S_c is the cross-sectional area of the chamber, and S_p is the cross-sectional area within a single perforate. The wave propagation within the single orifice is then computed using

$$\begin{pmatrix} p_3 \\ u_3 \end{pmatrix} = \begin{pmatrix} T_{11} & T_{12} \\ T_{21} & T_{22} \end{pmatrix}\begin{pmatrix} p_2 \\ u_2 \end{pmatrix}, \tag{6}$$

where d_c is equal to the orifice diameter in the calculation of the shear wave number. Again, the acoustic pressure and acoustic mass flow are assumed to be constant across the $\{3, 4\}$ interface, such that $p_4 = p_3$ and $S_c u_4 = N_p S_p u_3$.

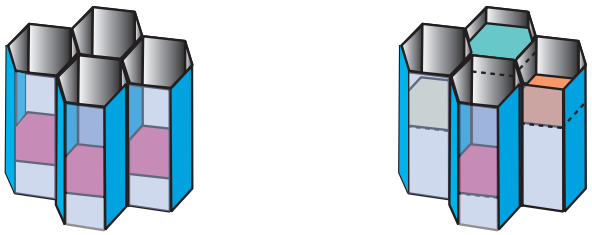
The normalized surface admittance for the individual chamber (the portion between points 'A' and 'B' in Figure 2) is computed as $\beta_c = u_4/p_4$. Assuming the liner is comprised of multiple chambers, the effective admittance across the liner surface is given by $\beta_s = \sum_{i=1}^{N_c} \Omega_i \beta_{c,i}$, where N_c is the number of chambers that combine to form the liner and Ω_i and $\beta_{c,i}$ are the surface open area ratio and surface admittance of the i^{th} chamber, respectively. The uniform, effective, surface impedance of the liner is then given by $\zeta_s = 1/\beta_s$.

3. VARIABLE-IMPEDANCE LINER CONCEPTS

3.1. MDOF Liners with Embedded Mesh Caps

Conventional 2DOF liners are comprised of a uniform depth core in which the upper and lower portions of the core are separated by a septum, typically either a perforated sheet or wire mesh. This causes the liner to absorb sound over a wider frequency range than can be achieved with SDOF liners (uniform core, no septum), but tends to reduce the peak attenuation. There are three tuning frequencies for a 2DOF liner, one for each of the frequencies with quarter-wavelengths corresponding to the upper, lower, and total core depths.

The broadband sound absorption properties of 2DOF liners can be further improved by allowing the properties of the embedded septum - penetration depth and DC flow resistance - to vary for the individual chambers that make up the liner core (see Figure 3; different colors are used to indicate distinct DC flow resistances). This causes the number of degrees of freedom to grow (labeled as multidegree-of-freedom, or MDOF), thereby allowing for better control of the acoustic properties over a wider range of frequencies. The NASA team has conducted a number of tests [6, 9–13] using MDOF samples fabricated by the Hexcel Corporation [14], most with two but some with three layers (two septa per core chamber).



(a) 2DOF core. (b) MDOF core.

Figure 3: Four chambers of two-layer liner cores with embedded mesh caps.

Figure 4 presents a comparison of predicted (using ZKTL model) and measured absorption coefficient spectra for an MDOF liner. This particular liner consists of two distinct chambers that are replicated throughout the volume of the liner. The penetration heights (distance from backplate to embedded mesh-cap) are 37.3 and 21.6 mm, respectively, and the corresponding septa DC flow resistances are 280 and 590 MKS Rayls. A 150 MKS Rayl wire mesh facesheet is also included and the total liner thickness is 43.2 mm. The comparison is favorable for frequencies up to about 2000 Hz, but the measured absorption is overpredicted for the higher frequencies.

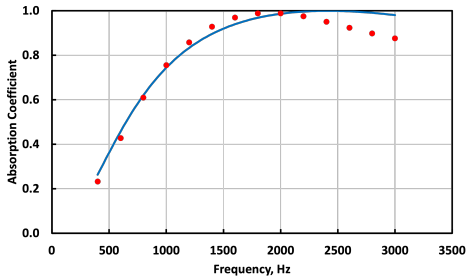


Figure 4: Comparison of predicted (blue line) and measured (red circles) absorption coefficient spectra for an MDOF core with a wire mesh facesheet.

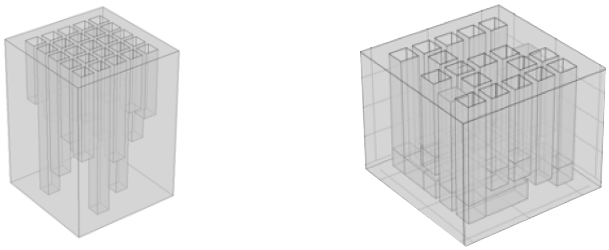
3.2. Variable Depth Liners

Variable-depth liners [6] (see Figure 5) have been studied for nearly five decades and are finally becoming more viable for aircraft applications due to recent advances in additive manufacturing (3D printing). The individual core chambers have different depths, such that each chamber may be tuned (quarter-wavelength resonator) to a different frequency. By judicious selection of the different chamber depths, the liner can be designed to absorb sound over a wide frequency range. Although the frequency tuning is dominated by the choice of chamber depths, the majority of the acoustic resistance is achieved via the perforated facesheet.

Two configurations are presented in Figure 5, one with straight chambers and the other with bent chambers. Bent chambers can be packed more efficiently, thereby allowing the frequency range of absorption to be extended to lower frequencies than possible with simple SDOF and 2DOF configurations.

The ZKTL model is used to compute impedances for variable-depth liners with either straight or bent chambers. Each chamber is evaluated independently, and the results are combined to get an effective distributed impedance. In cases where there is tangential flow over the surface, ZKTL is used to compute the core impedance and TPM is used to compute the impedance change across the facesheet.

The length of a bent chamber can be predicted (via ZKTL) as the sum of the individual segments that make up the chamber. However, this neglects the effects of nonuniform acoustic pressure and changing propagation wavenumbers through the bends. It should be noted that Cummings [15] offers an approach to account for bends in the impedance computation. The key parameters are the radius of curvature and angle of the bend. Interestingly, the choice of these two parameters can cause the effective chamber length to be either shorter or longer than the actual chamber length (as measured along the centerline). However, properly accounting for these bends becomes more difficult as the number and angles of bends increases. It should also be noted that the impedances of these configurations can be more accurately predicted via higher-fidelity tools (e.g., COMSOL [16]). Regardless, the ZKTL model is sufficient for parameter studies.



(a) Straight chambers. (b) Bent chambers.

Figure 5: Variable-depth liner configurations; facesheet not shown.

One additional issue that must be considered when bent chambers are used is packaging. To use the available volume efficiently, it is often necessary to bend a single chamber in multiple directions (fully 3D configuration). A useful tool, Packing3D [17], has been developed for this application. This code only allows for 90° or 180° bends in the individual chambers, but can very quickly combine chambers of variable lengths (depths) to fit into the available volume. For example, packaging of a 25-chamber configuration that includes five unique chamber depths can be achieved in a few seconds.

Figure 6 provides a comparison of predicted and measured absorption spectra for straight and bent-chamber liners based on a configuration similar to that shown in

Figure 5, with chamber lengths of 39, 71, and 123 mm (no facesheet). Total thicknesses are 127 mm and 66 mm, respectively, for the straight and bent-chamber liners. The measured results are very similar for the straight and bent-chamber configurations, and the comparison with predicted results is also quite favorable. This indicates the choice of straight or bent chambers has limited effect on the acoustic performance. The orange dashed trace on this figure depicts the predicted effects of adding a facesheet with a normalized resistance of 0.9 over the surface of the liner. This causes the predicted absorption coefficient spectrum to have much higher and broader peaks. The valleys in the absorption spectrum could have higher absorption coefficient values by inclusion of additional chamber depths.

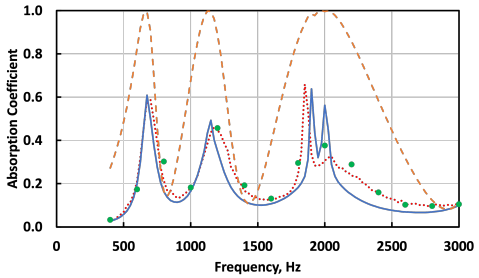


Figure 6: Comparison of predicted and measured absorption spectra. Measured bent- and straight-chamber results (with no facesheet) are represented with green circles and red dotted lines, respectively. Predicted results (assuming straight-chamber configuration) are represented with blue lines (no facesheet) and orange dashed lines (with facesheet).

3.3. Shared inlet port

The shared inlet port configuration [18] offers a twist on the variable-depth concept. One implementation is shown in Figure 7. Part (a) of the figure presents a conventional variable-depth configuration, and part (b) presents a shared inlet configuration with the same individual chamber lengths. Two distinct chambers feed into the facesheet via a single port that has similar cross-sectional geometry to that of a single chamber. In other words, the portion of the core that communicates with the impinging sound wave via the facesheet is roughly half the size of that for the conventional liner. As a side benefit, the resultant reduced surface porosity causes the liner drag to be reduced.



(a) Conventional. (b) Shared inlet port.

Figure 7: Conventional and shared inlet port liner configurations.

Figure 8 provides an absorption coefficient spectrum measured with a 43 mm-thick liner similar to that shown in Figure 7(b), with eight chambers of different depths combined as pairs at their joined surfaces. Each chamber depth produces increased absorption at or near its respective quarter-wavelength (seven are observed; one is outside the displayed frequency range). There are distinct dips in the absorption when two adjacent tuning frequencies are sufficiently far apart, slightly more so than for the case of conventional variable-depth liners (not shown), but the broadband absorption remains significant.

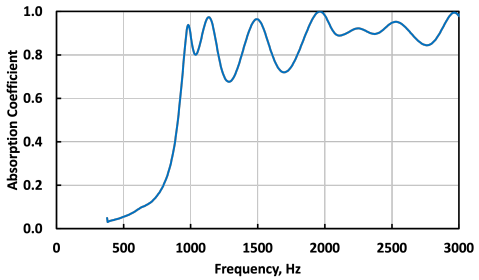


Figure 8: Measured absorption coefficient spectrum for a shared inlet port liner.

3.4. Variable facesheet

Variable facesheet liners (see Figure 9) are essentially the same as conventional SDOF liners, except the geometric properties of the facesheet (perforate hole diameter, open

area ratio, and facesheet thickness) are allowed to vary from chamber to chamber. Until recently, it was difficult (and costly) to consider using facesheets for which these properties varied rapidly over the surface of the liner. However, additive manufacturing and robotic drilling processes allow for straightforward implementation of the variable facesheet concept. If the facesheet geometric properties are allowed to be different for adjacent chambers, the resultant distributed impedance can be tuned to achieve desired absorption spectra. An earlier study [19] has shown that proper distribution of the geometric properties over the surface of a liner can be used to achieve significant broadband noise reduction relative to what could be achieved with a uniform facesheet.



(a) Wide chamber core.

(b) Variable facesheet.

Figure 9: Sketch of core (a) and variable facesheet (b) liner configurations.

Measured absorption spectra for a 38.1 mm-thick, variable facesheet liner are presented in Figure 10. Although there are clear effects of source level, the liner provides significant broadband absorption. These results provide evidence of the value of this concept, but investigation to optimize the configuration are needed.

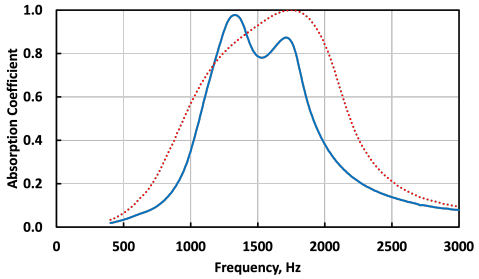


Figure 10: Measured absorption spectra for a variable facesheet liner at source levels of 120 dB (blue solid line) and 140 dB (red dotted line).

4. CONCLUDING REMARKS

This paper presented predicted and measured results for four variable-impedance liner concepts investigated at the NASA Langley Research Center. Each of these liner concepts can be designed to achieve sound absorption over a wide frequency range and can also be tuned for increased absorption at selected frequencies. These concepts include a modified version of a conventional two-layer liner, two types of variable-depth liners, and a variable-facesheet liner. Data acquired in the NASA normal incidence and grazing flow impedance tubes were used to demonstrate the capabilities of these concepts.

ACKNOWLEDGEMENTS

The author gratefully acknowledges the contributions of the NASA Langley Research Liner Physics Team. Special thanks are due to Brian Howerton for work on variable-depth liners, Noah Schiller for development of the shared inlet port concept, Martha Brown for investigation of the variable facesheet configuration, and Alonzo (Max) Reid for test support.

REFERENCES

[1] U. Ingard. On the theory and design of acoustic resonators. *Journal of the Acoustical Society of America*, 25:1037–1061, 1953.

[2] D. T. Blackstock. *Fundamentals of Physical Acoustics*. Wiley, 2000.

[3] R. E. Motsinger and R. E. Kraft. Design and performance of duct acoustic treatment: Aeroacoustics of flight vehicles; chapter 14, vol. 2: Noise control. NASA RP 1258, August 1991.

[4] T. L. Parrott and M. G. Jones. Assessment of nasa's aircraft noise prediction capability, chapter 6: Uncertainty in acoustic liner impedance measurement and prediction. NASA TP 2012-215653, July 2012.

[5] T. L. Parrott and M. G. Jones. Parallel-element liner impedances for improved absorption of broadband sound in ducts. *Noise Control Engineering Journal*, 43(6), November 1995.

[6] M. G. Jones, B. M. Howerton, and E. Ayle. Evaluation of parallel-element, variable-impedance, broadband acoustic liner concepts. AIAA Paper 2012-2194, June 2012.

[7] C. Zwikker and C.W. Kosten. *Sound absorbing materials*. Elsevier Publishing Company, 1949.

[8] H. Tijdeman. On the propagation of sound waves in cylindrical tubes. *Journal of Sound and Vibration*, 39(1):1–33, 1975.

[9] D. M. Nark and M. G. Jones. Broadband liner optimization for the source diagnostic test fan. AIAA Paper 2012-2195, June 2012.

[10] D. M. Nark, M. G. Jones, and D. L. Sutliff. Further development and assessment of a broadband liner optimization process. AIAA Paper 2016-2784, May 2016.

[11] M. G. Jones, D. M. Nark, A. Baca, and C. R. Smith. Applications of parallel-element, embedded mesh-cap, acoustic liner concepts. AIAA Paper 2018-3445, June 2018.

[12] D. M. Nark, M. G. Jones, N. H. Schiller, and D. L. Sutliff. Broadband inlet liner design for the dgen aeropropulsion research turbofan. AIAA Paper 2018-3608, June 2018.

[13] D. L. Sutliff, D. M. Nark, M. G. Jones, and N. H. Schiller. Design and acoustic efficacy of a broadband liner for the inlet of the dgen aero-propulsion research turbofan. AIAA Paper 2019-2582, May 2019.

[14] E. Ayle. Acoustic septum honeycomb. U.S. Patent 2011/0073407A1, March 2011.

[15] A. Cummings. Sound transmission in curved duct bends. *Journal of Sound and Vibration*, 35(4):451–477, 1974.

[16] Comsol acoustic module user's guide. v5.1, 2015.

[17] M. M. Marinova, M. G. Jones, and N. H. Schiller. Evaluation of packing3d code for design of variable-depth, bent-chamber acoustic liners. NASA TM 220560, February 2020.

[18] N. H. Schiller, M. G. Jones, B. M. Howerton, and D. M. Nark. Developments of a low-drag variable-depth acoustic liner. AIAA Paper 2019-2749, May 2019.

[19] M. C. Brown and M. G. Jones. Evaluation of variable facesheet liner configurations for broadband noise reduction. AIAA Paper 2020-2616, June 2020.